Received: 9 February 2024 | Revised: 30 March 2024 | Accepted: 3 April 2024

DOI: 10.1002/ardp.202400115

FULL PAPER

ARCH PHARM DPhG
Archiv der Pharmazie

Design and synthesis of phenoxy methyl-oxadiazole compounds against Alzheimer's disease

Asaf E. Evren[1,2] | Demokrat Nuha[1,3] | Begüm N. S. Özkan[1] | Çiğdem Kahraman[4] | Ekrem M. Gönülalan[5] | Leyla Yurttaş[1]

[1]Department of Pharmaceutical Chemistry, Faculty of Pharmacy, Anadolu University, Eskişehir, Turkey

[2]Vocational School of Health Services, Department of Pharmacy Services, Bilecik Şeyh Edebali University, Bilecik, Turkey

[3]Faculty of Pharmacy, University for Business and Technology, Prishtina, Kosovo

[4]Department of Pharmacognosy, Faculty of Pharmacy, Hacettepe University, Ankara, Turkey

[5]Department of Pharmacognosy, Faculty of Pharmacy, Afyonkarahisar Sağlık Bilimleri University, Afyon, Turkey

Correspondence
Demokrat Nuha, Faculty of Pharmacy, University for Business and Technology, Prishtina, Kosovo.
Email: demokratnuha@gmail.com and demokrat.nuha@ubt-uni.net

Funding information
None

Abstract

This study examines the synthesis and evaluation of 11 newly developed compounds as potential anti-Alzheimer's agents that occur via cholinesterase and β-secretase inhibition. The compounds were tested for their inhibitory activity against acetylcholinesterase (AChE) and butyrylcholinesterase (BChE) using the modified Ellman method. The results showed that several compounds exhibited significant inhibition of AChE, particularly compounds **6d**, **7a**, and **7e**, which demonstrated high inhibitory activity at lower concentrations, with IC_{50} values of 0.120, 0.039, and 0.063 µM, respectively. However, the compounds showed limited effectiveness against BChE, with only a few compounds exhibiting moderate inhibition. Compound **7e** showed an inhibitory effect against BACE-1 close to that of the standard drug. Structural analysis revealed that the compounds with substituted benzothiazole and thiazole moieties exhibited the most promising inhibitory activity. This study provides valuable insights into the potential of these synthesized derivatives as a treatment against Alzheimer's disease. Moreover, the structure, stability, and properties of the active compounds were further investigated using density functional theory calculations. As a final note, the utilization of molecular docking and molecular dynamics simulation studies allowed us to elucidate the action mechanism of the active compounds and gain insights into the structure–activity relationship against AChE and β-secretase proteins. These computational techniques provide valuable information on the binding modes, interactions with target enzymes, dynamic behavior, and conformational changes of the compounds, enabling a comprehensive understanding of their biological activity.

KEYWORDS
1,3,4-Oxadiazole, β-secretase, cholinesterase, molecular docking, molecular dynamics stimulation

1 | INTRODUCTION

Alzheimer's disease (AD) is a devastating neurodegenerative disorder and the most prevalent form of dementia, characterized by memory loss and cognitive decline. According to the World Alzheimer Report 2022, approximately 50 million people worldwide are affected by AD and related dementia, with an estimated 75% of cases going undiagnosed.[1,2] The impact of AD extends beyond the well-being of patients, as it also poses a significant economic burden projected to exceed 1 trillion dollars by 2050.[3,4]

The leading pathological pathways of AD, such as the amyloid-β (Aβ) and tau protein hypotheses, have been extensively studied. While various targeted small molecules are being evaluated in clinical trials, only five medications have been approved by the FDA: four acetylcholinesterase (AChE) inhibitors and one *N*-methyl-D-aspartate receptor antagonist.[5] The amyloid-β (Aβ) peptide is a key player in the pathogenesis of AD, as it tends to aggregate and form plaques in the brains of affected individuals. Such plaques are believed to contribute to neurodegeneration, a hallmark of AD. Consequently, inhibiting Aβ aggregation is considered a potential therapeutic strategy to mitigate AD progression.[6] BACE-1 (beta-secretase 1) is an enzyme involved in the production of Aβ peptides. Inhibiting BACE-1 activity can lead to a reduction in the production of Aβ peptides, addressing one of the early steps in the formation of amyloid plaques.[7] Therefore, compounds with BACE-1 inhibitory activity are of significant interest in the development of AD therapeutics. Although AChE inhibitors can provide temporary symptom relief by enhancing cholinergic receptors and improving memory function, they often lack efficacy in delaying disease progression and may cause undesirable side effects. Notably, there has been a dearth of new disease-modifying small molecular drugs approved in the past two decades, and the recent approval of aducanumab remains a topic of controversy.[8]

Given the complex and multifactorial nature of AD, there is growing interest in the development of multifunctional small molecules that target multiple pathways simultaneously. Butyrylcholinesterase (BChE), an enzyme involved in the hydrolysis of acetylcholine, has gained significance as a pharmacological target for AD.[9] Dual AChE and BChE inhibitors, such as hybrid compounds, have demonstrated promising effects, including antineuroinflammatory and neuroprotective properties.[10] Neuroinflammation, driven by activated microglia, is another key mechanism implicated in AD progression. Prolonged microglia activation leads to the release of inflammatory molecules like nitric oxide (NO) and pro-inflammatory cytokines, contributing to neurodegeneration.[11,12] Recent studies have highlighted the potential of multifunctional neuroprotective agents in reducing NO production, inhibiting AChE activity, and suppressing the expression of inflammatory markers.[13]

The development of more effective and curative therapeutics for AD remains an urgent priority. Multifunctional small molecules that target multiple pathways, including AChE, BChE, and neuroinflammation, offer a promising approach to the treatment of AD.[14,15] By addressing the complex nature of the disease, these compounds have the potential to provide comprehensive therapeutic benefits and improve the lives of individuals affected by AD.[16]

A series of oxadiazole, thiazole, and benzothiazole hybrids have emerged as promising multi-target compounds for the treatment of AD.[17] These compounds exhibit multi-target properties by influencing various pathological pathways associated with AD. This includes beta-amyloid inhibitory activity, where the hybrids effectively inhibit the aggregation of Aβ peptides, and BACE-1 inhibitory activity, whereby they act on the enzyme responsible for Aβ production.[18] Their unique chemical structures allow them to interact with key enzymes, such as AChE and BChE, thereby enhancing cholinergic function.[19] Additionally, these hybrids demonstrate anti-amyloidogenic properties by inhibiting Aβ aggregation and promoting its clearance. Furthermore, they exhibit anti-neuroinflammatory effects by suppressing the release of pro-inflammatory cytokines. The multitarget approach of these compounds holds promise for the development of effective therapeutics for AD.[20]

Our research was motivated by existing knowledge and aimed to create a unique set of compounds with physiological activity. The compounds synthesized in this study are hybrids of oxadiazole, thiazole, and benzothiazole. This article presents a thorough account of the experimental procedures, including synthesis and characterization, as well as the application of various computational techniques such as molecular docking, molecular dynamics simulation, and DFT calculations. Furthermore, the inhibitory effects of these compounds on cholinesterase enzymes were evaluated. The comprehensive methodologies and results obtained from these investigations are extensively discussed in this paper, providing valuable insights into the potential therapeutic applications of these compounds.

2 | RESULTS AND DISCUSSION

2.1 | Chemistry

The target compounds **6a–f** and **7a–e** were synthesized as shown in Scheme 1. At first, methyl 2-(2,4-dichlorophenoxy)acetate (**1**) was synthesized from 2-(2,4-dichlorophenoxy)acetic acid by esterification. Then, compound **1** was treated with hydrazine to gain 2-(2,4-dichlorophenoxy)acetohydrazide (**2**). 5-[(2,4-Dichlorophenoxy)methyl]-1,3,4-oxadiazole-2-thiol (**3**) was synthesized from compound **2** using carbon disulfide via ring closure. Benzothiazol-2-amine and thiazol-2-amine derivatives were acetylated to gain *N*-(benzothiazol-2-yl)-2-chloroacetamide derivatives (**4a–f**) and 2-chloro-*N*-(thiazol-2-yl) acetamide derivatives (**5a–e**). At the last step, compound **3** was treated with compounds **4a–f** and **5a–e** in acetone to obtain *N*-(benzothiazol-2-yl)-2-({5-[(2,4-dichlorophenoxy)methyl]-1,3,4-oxadiazol-2-yl}thio) acetamide derivatives (**6a–f**) and 2-({5-[(2,4-dichlorophenoxy)methyl]-1,3,4-oxadiazol-2-yl}thio)-*N*-(thiazol-2-yl)acetamide derivatives (**7a–e**) according to the S_N2 reaction. The structures of the synthesized compounds were confirmed by ^{1}H-NMR, ^{13}C-NMR, and high-resolution mass spectroscopy (HRMS). In the ^{1}H-NMR spectra of aromatic and aliphatic regions, the peaks were seen in estimated areas. The signals belonging to S-$\underline{CH_2}$ protons were observed at 4.19–4.45 ppm and signals belonging to O–$\underline{CH_2}$ were detected at 5.51–5.52 ppm as singlet peaks in common in the ^{1}H-NMR spectra of all compounds. Also, a broad singlet peak was seen at 12.66–12.71 ppm indicating the acetamide N–H proton, for all compounds. The appearance of a pair of singlet, doublet, triplet and/or multiplet at 6.78–8.82 ppm was due to the aromatic protons of the aromatic rings. In the ^{13}C-NMR spectra of

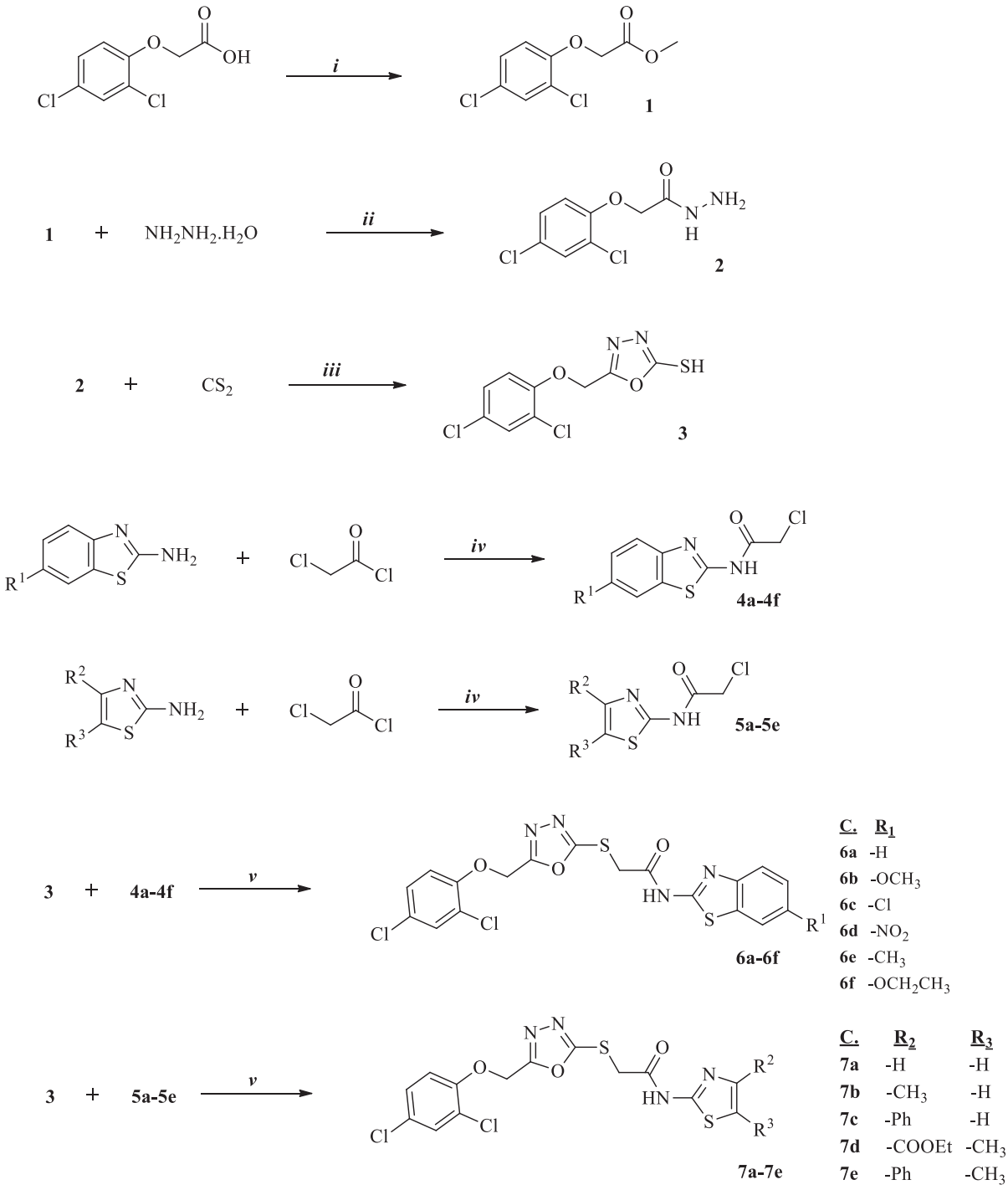

C.	R_1
6a	-H
6b	$-OCH_3$
6c	-Cl
6d	$-NO_2$
6e	$-CH_3$
6f	$-OCH_2CH_3$

C.	R_2	R_3
7a	-H	-H
7b	$-CH_3$	-H
7c	-Ph	-H
7d	-COOEt	$-CH_3$
7e	-Ph	$-CH_3$

SCHEME 1 The synthesis of the compounds. Reactants and conditions: (i) MeOH, H_2SO_4, 65°C, 72 h; (ii) EtOH, r.t.; (iii) KOH, EtOH, reflux, 6 h, then diluted HCl; (iv) TEA, THF, 0–5°C, (v) K_2CO_3, r.t.

compounds in the aromatic and aliphatic regions, peaks were seen at estimated areas and common signals at 35.99–40.10, 61.05–61.12, and 163.51–170.63 ppm were assigned to S-$\underline{CH_2}$ carbon, O-$\underline{CH_2}$ carbon, and carbonyl (C=O) carbon. The aromatic carbon signals were detected in the 105.17–167.39 ppm range. The mass spectra (ESI-MS) of the compounds showed that [M+1] peaks were in agreement with their calculated molecular weight of M±1.

2.2 | Biology

2.2.1 | Anticholinesterase activity

N-(Benzo/thiazol-2-yl)-2-({5-[(2,4-dichlorophenoxy)methyl]-1,3,4-oxadiazol-2-yl}thio)acetamide derivatives (**6a–f** and **7a–e**) were tested to determine AChE and BChE inhibitory activity according to

the modified Ellman method. The compounds were first tested at 10^{-3} and 10^{-4} M concentrations, those with inhibitions greater than 50% were studied at lower concentrations to determine IC_{50} values. Donepezil and tacrine were used as the standard drugs. The percent inhibitions and IC_{50} concentrations obtained are presented in Table 1. Also, the dose–response curves of the selected compounds and reference drugs are shown in Figure 1. Compounds **6b**, **6c**, **6d**, **6e**, **7a**, **7b**, and **7e** showed more than 50% inhibition of AChE at 10^{-3} M concentration, and only **6d** (85.718%), **7a** (95.923%) and **7e** (94.517%) compounds showed high inhibition at the lower concentration of 10^{-4} M, so the IC_{50} dose was calculated for these compounds. The IC_{50} values for compounds **6d**, **7a**, and **7e** were determined as IC_{50}: 0.120 µM, IC_{50}: 0.039 µM and IC_{50}: 0.063 µM, respectively. Among these compounds, compounds **7a** and **7e** were determined as the compounds showing the closest potential to donepezil (IC_{50}: 0.0201 µM) with the highest inhibition doses. When the inhibitory effects of the compounds on BChE were examined, it was found that only four compounds (**6c**, **6f**, **7a**, and **7b**) exhibited more than 40% inhibition at 10^{-3} M concentrations; It is seen that the compounds remained in inhibition of 32% at a concentration of 10^{-4} M. According to this result, it can be said that the compounds are ineffective against BChE.

When the compounds are evaluated in terms of chemical structure, it is seen that **6a–f** compounds contain substituted benzothiazole, and **7a–e** compounds contain substituted thiazole. While the most active derivative was found to contain 6-nitro substituent (**6d**) among compounds **6a–f**; nonsubstituted thiazole derivatives (**7a**) and 4-phenyl-5-methyl substituents containing derivatives (**7e**) showed the highest inhibitory activity in those containing thiazole (**7a–e**).

2.2.2 | β-Secratase inhibition

Table 2 shows IC_{50} values of the β-secretase enzyme. According to the results, compound **6d** did not inhibit enzymes at a 10 µM concentration. Compound **7a** has half the potency of **7e** and donepezil. On the other hand, compound **7e** has a potency that is close to donepezil, however, its potency is not higher than verubecestat. These findings indicated that the condensed ring system such as benzothiazole (**6d**) is not favored, on the contrary, the mono ring system, thiazole, showed inhibitory activity. Specifically, when the substituents on the thiazole ring are at the fourth and fifth positions (**7e**) or there is no group (**7a**) at these positions, inhibitory potency is observed. To understand the binding modes, and also clarify the SARs, in silico studies were run.

2.3 | ADME prediction

Table 3 displays the predicted computational results. There was no violation of Lipinski's rule of five[21] based on these findings. These results are consistent with the compounds' activity potential. The synthesized molecules are expected to have a favorable pharmacokinetic profile. As a result, the compounds' drug-likeness was assigned a positive value. Log P of the compounds was between 3.07 and 4.88. TPSA is predicted between the range of 143.68–189.50. The number of HBA was calculated as 6–8, HBD as 1 for all compounds. All of the compounds are slightly soluble in water because log S < −6 and they have low absorption in the gastrointestinal tract. Synthetic accessibility was predicted in between 3.42 and 3.72 which was evaluated 1—*very easy* to 10—*very difficult*.

TABLE 1 % Inhibition rates and IC_{50} (µM) values of the obtained compounds against acetylcholinesterase (AChE) and butyrylcholinesterase (BChE) enzymes at 10^{-3} and 10^{-4} M concentrations.

	AChE İnhibition %			BChE İnhibition%		
Bileşik	10^{-3} M	10^{-4} M	AChEIC_{50} (µM)	10^{-3} M	10^{-4} M	BChEIC_{50} (µM)
6a	46.641 ± 0.907	39.026 ± 0.810	>1000	31.821 ± 0.921	23.361 ± 0.753	>1000
6b	63.026 ± 1.352	41.684 ± 1.162	>100	30.163 ± 1.274	20.427 ± 0.885	>1000
6c	74.831 ± 2.087	48.069 ± 0.936	>100	42.648 ± 1.8	28.749 ± 0.967	>1000
6d	91.499 ± 2.744	85.718 ± 2.536	0.120 ± 0.005	36.295 ± 1.155	29.137 ± 0.930	>1000
6e	79.286 ± 2.157	36.649 ± 0.826	>100	39.412 ± 1.374	21.052 ± 0.858	>1000
6f	44.511 ± 0.923	40.575 ± 1.135	>1000	44.937 ± 1.878	24.508 ± 0.937	>1000
7a	98.158 ± 2.726	95.923 ± 1.855	0.039 ± 0.001	41.066 ± 0.912	26.667 ± 0.887	>1000
7b	52.066 ± 1.634	21.496 ± 0.979	>100	47.307 ± 1.253	32.241 ± 1.190	>1000
7c	38.321 ± 1.028	23.250 ± 0.855	>1000	30.749 ± 0.947	21.837 ± 0.920	>1000
7d	40.558 ± 0.932	26.312 ± 0.874	>1000	36.231 ± 1.052	31.722 ± 0.816	>1000
7e	96.799 ± 2.037	94.517 ± 2.408	0.063 ± 0.003	35.557 ± 1.042	27.941 ± 0.833	>1000
Donepezil	99.156 ± 1.302	97.395 ± 1.255	0.0201 ± 0.0010	95.623 ± 2.054	91.022 ± 1.668	0.1025 ± 0.0042
Tacrine	99.262 ± 2.415	98.547 ± 1.623	0.3624 ± 0.0129	99.827 ± 1.378	98.675 ± 1.450	0.0064 ± 0.0002

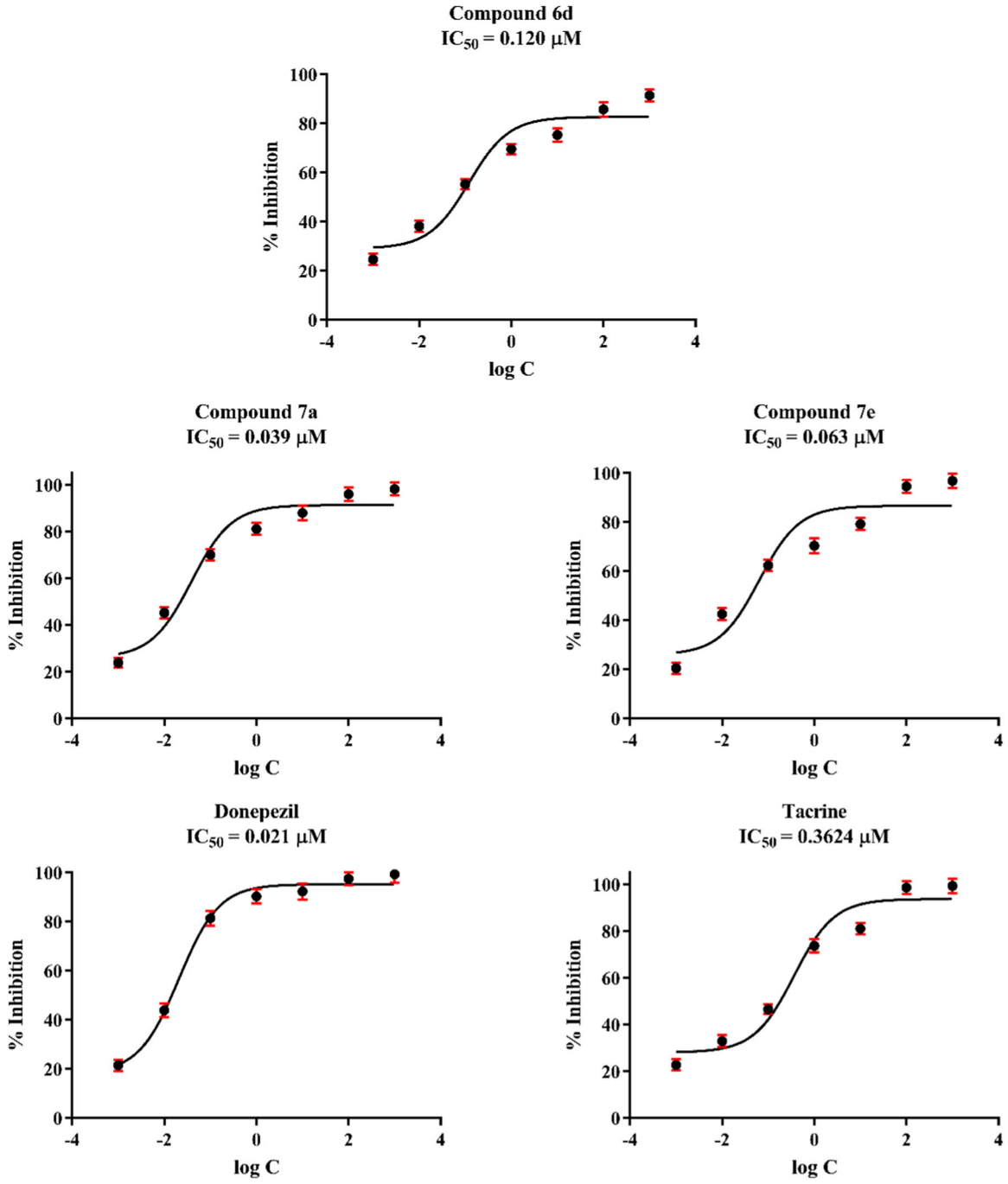

FIGURE 1 The IC_{50} graphs of compounds **6d**, **7a**, **7e**, donepezil and tacrine against acetylcholinesterase enzyme.

TABLE 2 IC_{50} (µM) values of the obtained compounds against BACE-1 enzymes.

Compounds	β-Secretase (BACE-1) IC_{50} (µM)
6d	>10
7a	0.204 ± 0.010
7e	0.123 ± 0.005
Donepezil	0.110 ± 0.005
Verubecestat	0.031 ± 0.001

The prediction model examines the relationship between the polarity and lipophilicity of compounds and their permeability through the blood–brain barrier (BBB). Since the drugs developed in this study target AChE in the central nervous system, it's crucial for them to have high or increased BBB permeability, indicating CNS penetration. One approach to enhance the bioavailability of loading molecules (**6a–f**, **7a–e**) in the CNS is by transporting them through the BBB using drug transport substrates. Nanotechnology has been utilized to devise strategies for medication delivery, effectively tackling various bioavailability challenges. In addition to lipophilicity,

TABLE 3 Physicochemical, pharmacokinetic, and medicinal chemistry properties of the final compounds (by SwissAdme) (**6a–f**, **7a–e**).

	Physicochemical properties						Pharmacokinetics		Medicinal chemistry	
	HBA	HBD	TPSA	Log $P_{o/w}$	Log S	GIA	Log K_p	BBB perm.	RoF (V)	SA
6a	6	1	143.68	4.30	−7.81	Low	−5.57	No	Yes (0)	3.42
6b	7	1	152.91	4.27	−7.97	Low	−5.77	No	Yes (0)	3.61
6c	6	1	143.68	4.77	−8.45	Low	−5.34	No	Yes (1)	3.48
6d	8	1	189.50	3.45	−8.58	Low	−5.97	No	Yes (1)	3.59
6e	6	1	143.68	4.59	−8.18	Low	−5.40	No	Yes (0)	3.47
6f	7	1	152.91	4.58	−8.35	Low	−5.60	No	Yes (1)	3.72
7a	6	1	143.68	3.07	−6.32	Low	−6.28	No	Yes (0)	3.24
7b	6	1	143.68	3.53	−6.74	Low	−6.08	No	Yes (0)	3.35
7c	6	1	143.68	4.51	−8.05	Low	−5.56	No	Yes (0)	3.57
7d	8	1	169.98	3.80	−7.86	Low	−6.13	No	Yes (1)	3.79
7e	6	1	143.68	4.88	−8.46	Low	−5.36	No	Yes (1)	3.71
RF-1	4	0	38.77	4.00	−4.81	High	−5.58	Yes	Yes (0)	3.36
RF-2	1	1	38.91	2.59	−3.18	High	−5.59	Yes	Yes (0)	2.91

Abbreviations: HBA, H-bond acceptor; HBD, H-bond donor; TPSA, topologic polar surface area (Å²); Log $P_{o/w}$, *Consensus* Log $P_{o/w}$ (average of all five predictions); Log S, water solubility; GIA, gastrointestinal absorption; Log K_p, skin permeation (cm/s); BBB perm., Blood–brain barrier permeability; RoF (V), rule of five (violation number); SA, synthetic accessibility from 1 (very easy) to 10 (very difficult); RF-1, Donepezil; RF-2, Tacrine.

the substances (**6a–f**, **7a–e**) exhibited topological polar surface areas (TPSA) that suggested inadequate BBB permeability.

2.4 | Results of DFT studies

The investigation of the structure, stability, and properties of the active compounds **6d**, **7a**, and **7e** involved the use of DFT-based global reactivity descriptors, which have been widely employed to determine the reactivity and site selectivity of various biomolecules. To examine the three-dimensional structure of the compounds, theoretical approaches were employed to generate optimized molecular structures. By conducting DFT optimization using the B3LYP/6-31G (d, p) basis set, the structures of the most active compounds (**6d**, **7a**, and **7e**), were obtained, and no imaginary frequency was observed. Figure 2 illustrates the optimized structures of these active compounds.

At the B3LYP/6-31G (d, p) level, the frontier molecular orbitals of the optimized geometries were analyzed. The energy difference between the highest occupied molecular orbital (HOMO) and the lowest unoccupied molecular orbital (LUMO) is crucial for determining chemical reactivity, optical polarizability, chemical softness, hardness, and molecular electrical transport properties of a chemical system.[22] Table 4 presents the energies of the frontier molecular orbitals and the energy difference between HOMO and LUMO. The negative HOMO and LUMO values indicate stability for compounds **6d**, **7a**, and **7e** (Figure 3). Experimental observations align with the chemical properties outlined in Table 4, suggesting that compound **6d** exhibits higher activity compared to the other compounds. Additionally, compound **7e** demonstrates a low ionization potential (I), while **6d** displays a high electron affinity (A), both attributed to their HOMO and LUMO energies. As a result, compound **7e** exhibits nucleophilic character, whereas the **6d** molecule demonstrates enhanced electrophilic character.

Electronegativity (χ) represents the ability of an atom or substituent group to attract shared electrons or electron density. A higher electronegativity value indicates a stronger electron attraction. Conversely, electro-positivity reflects a molecule's tendency to donate valence electrons. Among the examined compounds, compound **6d** stands out with an electronegativity value of 0.1644 eV, indicating higher electronegativity, and a better nucleophilic character than the other compounds. Furthermore, the chemical hardness-softness (η, *S*) values play a role in evaluating intramolecular charge transfer within molecular structures. Notably, compound **6d** demonstrates high softness (*S*) and low hardness (η) values, indicative of its distinct characteristics.

The analysis of molecular electrostatic potential (MEP) plays a crucial role in determining the charge distribution (positive and negative) within three-dimensional molecules and evaluating ligand binding and hydrogen bonding with biomolecules.[23] Figure 4 illustrates the MEP mapping results for the active compounds. MEP visualization utilizes a color scheme where red indicates areas with a partial negative charge and an electron-rich nature, blue represents regions with a partial positive charge and an electron-deficient nature, yellow signifies moderately electron-rich regions, and green indicates neutral regions.[24]

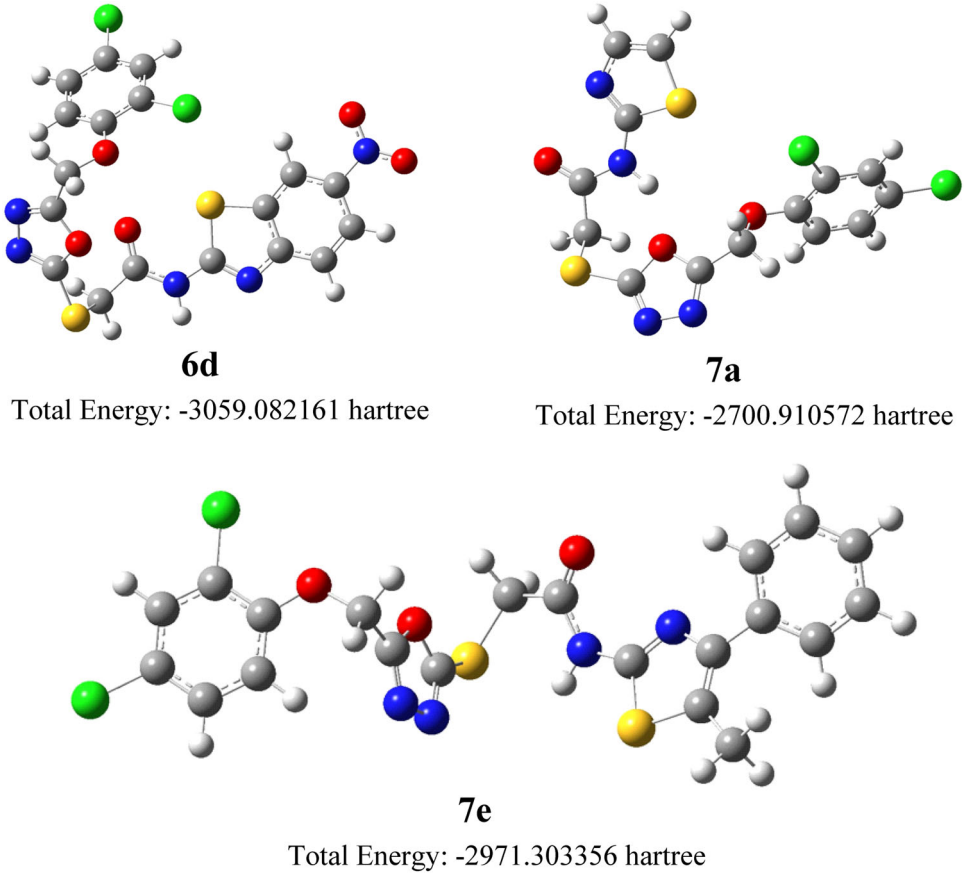

FIGURE 2 Optimized molecular structures and total energy values of active compounds.

TABLE 4 Some reactivity parameters of the most active compounds.

Compounds	E_{HOMO} (eV)	E_{LUMO} (eV)	ΔE (eV)	I (eV)	A (eV)	χ (eV)	η (eV)	S (eV^{-1})	μ (eV)	ω (eV)
6d	−0.2362	−0.0927	0.1435	0.2362	0.0927	0.1644	0.0717	6.9686	−0.1644	0.1884
7a	−0.2285	−0.0574	0.1711	0.2285	0.0574	0.1429	0.0855	5.8445	−0.1429	0.1194
7e	−0.2145	−0.0541	0.1604	0.2145	0.0541	0.1343	0.0802	6.2344	−0.1343	0.1124

2.5 | Molecular docking studies

2.5.1 | AChE inhibitory activity

After determination of active compounds (6d, 7a, and 7e) and their stable conformers via DFT calculations, the docking studies were performed in active pockets of AChE and BACE-1 enzymes.

According to Figure 5, the docking results indicated that the 2,4-dichlorophenoxy moiety of ligands localizes very similarly via interacting with CAS residues, Trp86 (π–π stacking), and Gly120 (halogen bond). Additionally, (benzo)thiazole moiety of the ligands interacted with the PAS region of the enzyme, Trp286 (π–π stacking) while oxadiazole ring was stacked with alfa-helix residues (seq. 335–342), specifically, these residues are Tyr337, Phe338, or Tyr341. The similarity of poses points out that the major player is 2,4-dichlorophenoxy moiety since this was bonding CAS region, however, oxadiazole ring protect probably forms stability of the ligand-protein complex. Moreover, (benzo)thiazole moiety has a direct effect on interactions of the PAS region while (benzo)thiazole also determines the most stable conformer in the binding pocket which also affects the complex stability. Also, acetamide moiety of the compounds commonly interacted with loop region (seq. 289–311) residues such as Phe295 and Phe297, means that this moiety has a positive impact on the complex stability. Compound **6a** and **7e** interacted with Ser203 while **7a** formed halogen bond with Ser125 and Tyr133. Specifically, only **6a** has additional interaction with Ser293 which is a member of the PAS residue. On the other hand, since (benz)azole residues of the compounds are localized in the entrance cavity (PAS) of the binding site, they were under solvent exposure, thus, we point out that this side was a determiner of secondary features such as physicochemical properties. Briefly, considering all these findings, we concluded that 2,4-dichlorophenoxy moiety has an important role in

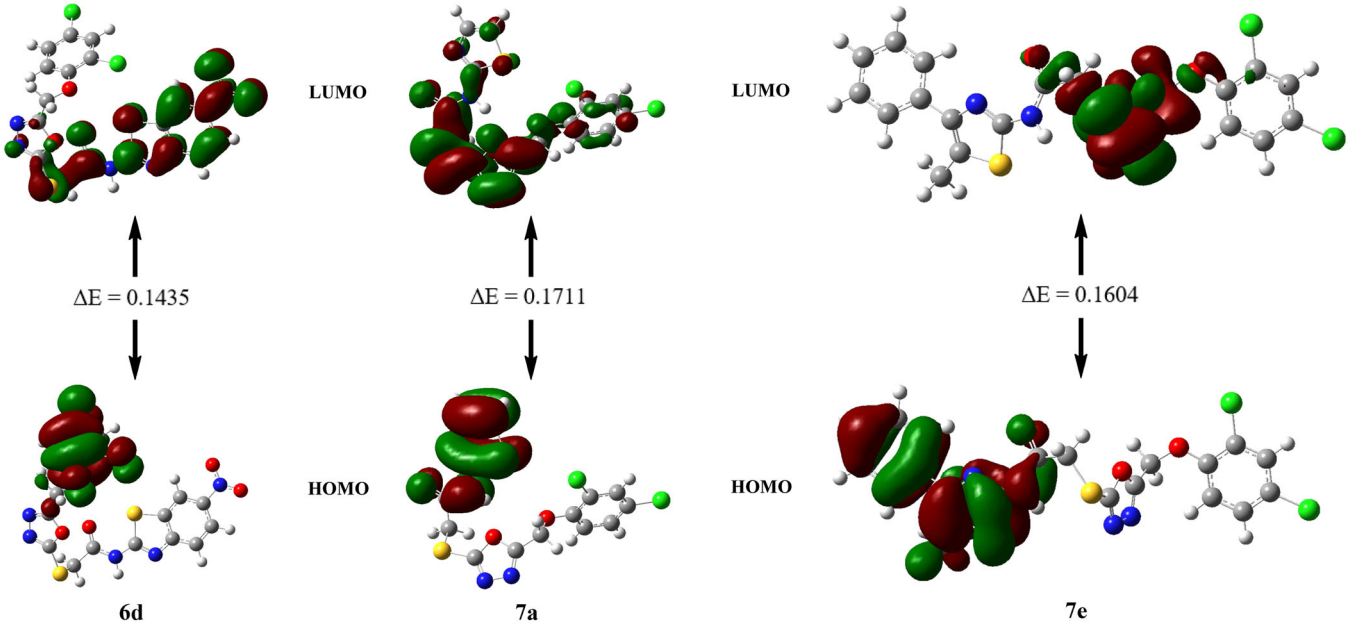

FIGURE 3 Highest occupied molecular orbital (HOMO)-lowest unoccupied molecular orbital (LUMO) diagrams of the active compounds.

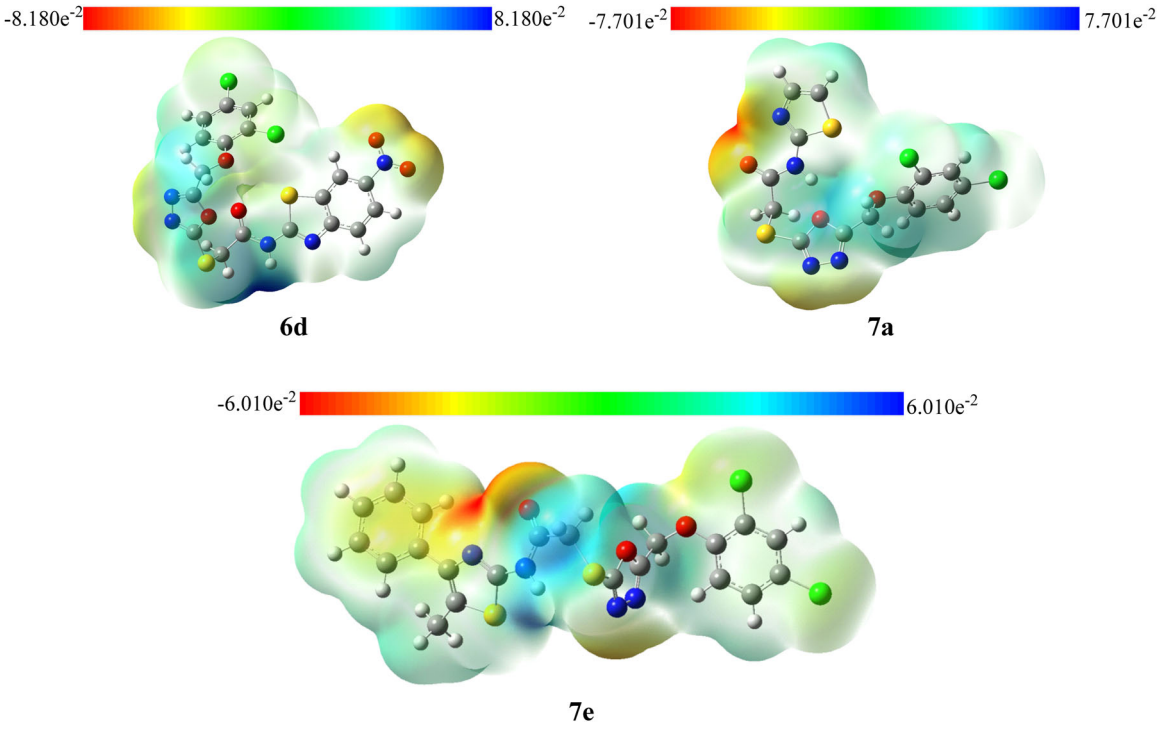

FIGURE 4 Molecular electrostatic potential surfaces presentation of the active compounds.

docking to the active cavity while the oxadiazole ring increases the stability of the complex. Indeed, these findings and previous reports are in harmony.[25–28] However, we also wanted to investigate complex stability versus time and environmental changes such as water and electrolytes, hence, molecular simulation study was run for the most active compound **7a**.

2.5.2 | BACE-1 inhibitory activity

The most active molecule was stated as **7e** via in vitro enzyme study, thus, molecular docking study was run to understand the possible binding mode on BACE-1 protein for this compound. The results were shared as 2D and 3D poses in Figure 6.

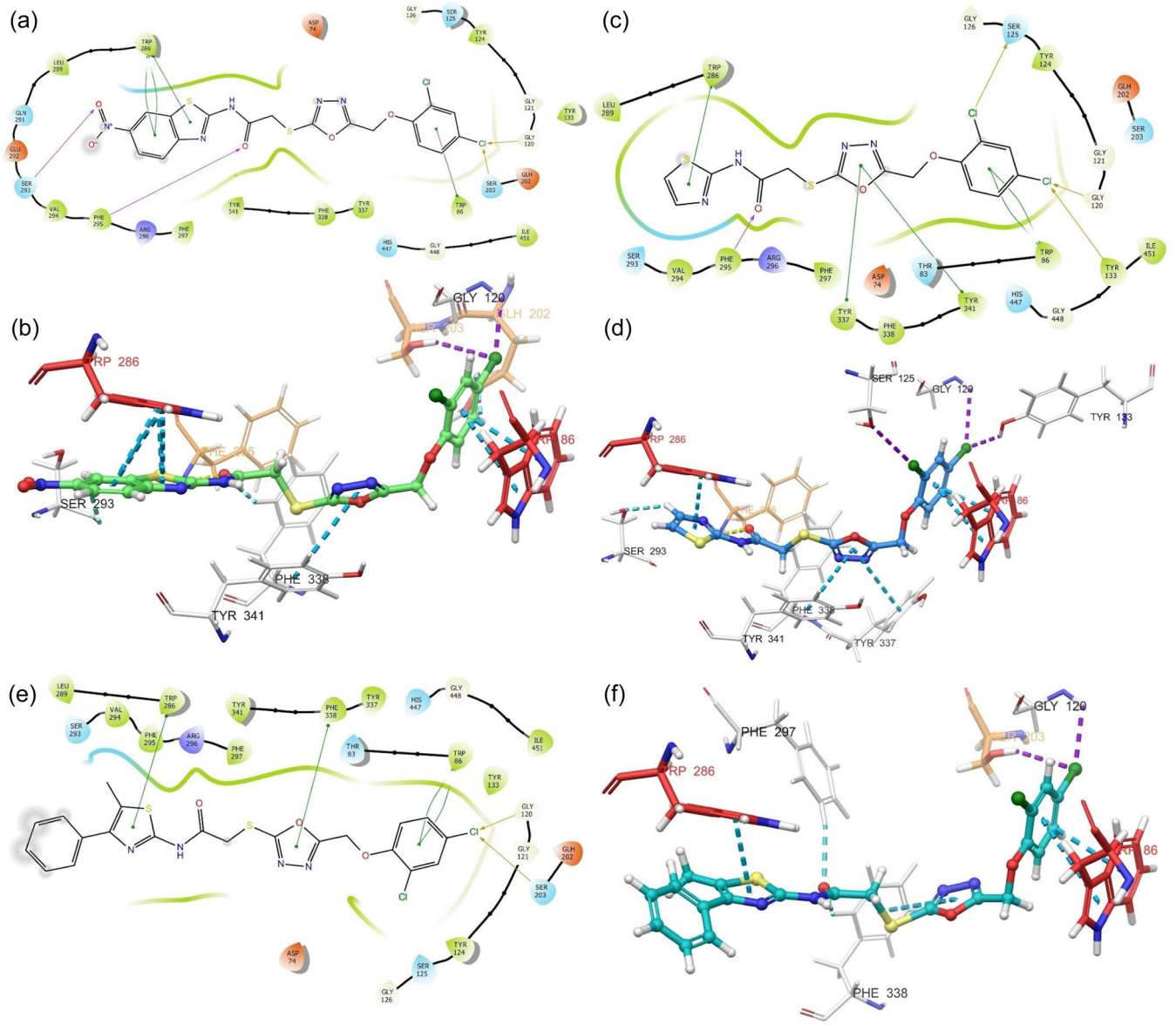

FIGURE 5 Best docking poses of compounds **6d**, **7a**, and **7e** in active cavity of the acetylcholinesterase (AChE) enzyme (PDBID: 4EY7). (a) 3D and (b) 2D poses of **6d**-AChE complex; (c) 3D and (d) 2D poses of **7a**-AChE complex; (e) 3D and (f) 2D poses of **7e**-AChE complex. For clarity, only interacted residues were shown. Red carbons represent key residues, other binding residues have white carbons.

It was indicated that acetamide moiety was very interesting position that laid out between Asp32 and Thr72 which are catalytic cleft residues. Also, the thiazole ring localized in the S1 pocket of the catalytic cleft, and phenyl and methyl moieties of this ring occupied this pocket very well. Additionally, phenyl hydrogen formed an aromatic H-bond with Gly11. Because of these reasons, we suggest that *N*-(4-phenyl-5-methyl-2-thiazolyl)-acetamide is a good pharmacophore structure that fulfills the active pocket. Also, oxadiazole formed H-bonds with Tyr71 and Tyr198 which are two different loop aminoacids, meanwhile, 2,4-dichlorophenoxy group rotated to Ser36 and Asn37 residues and formed halogen bonds. Thus, we thought that phenoxy and oxadiazole moieties increase the stability of the complex together. All these interactions clarified how **7e** docks to BACE-1 enzyme and why it has an inhibitory effect. However, to understand this relationship deeply from various perspectives, we also run a molecular dynamics simulation for **7e**-protein complex.

2.6 | Molecular dynamic studies

2.6.1 | AChE inhibitory activity

The results of the stability properties (Figure 7a–c) and binding modes (Figure 7d–f and in Video S1) were displayed. The fluctuations in the plot of radius of gyration (rG) were measured as ±1 Å. Root-mean-square deviation (RMSD) plots showed the highest peak is

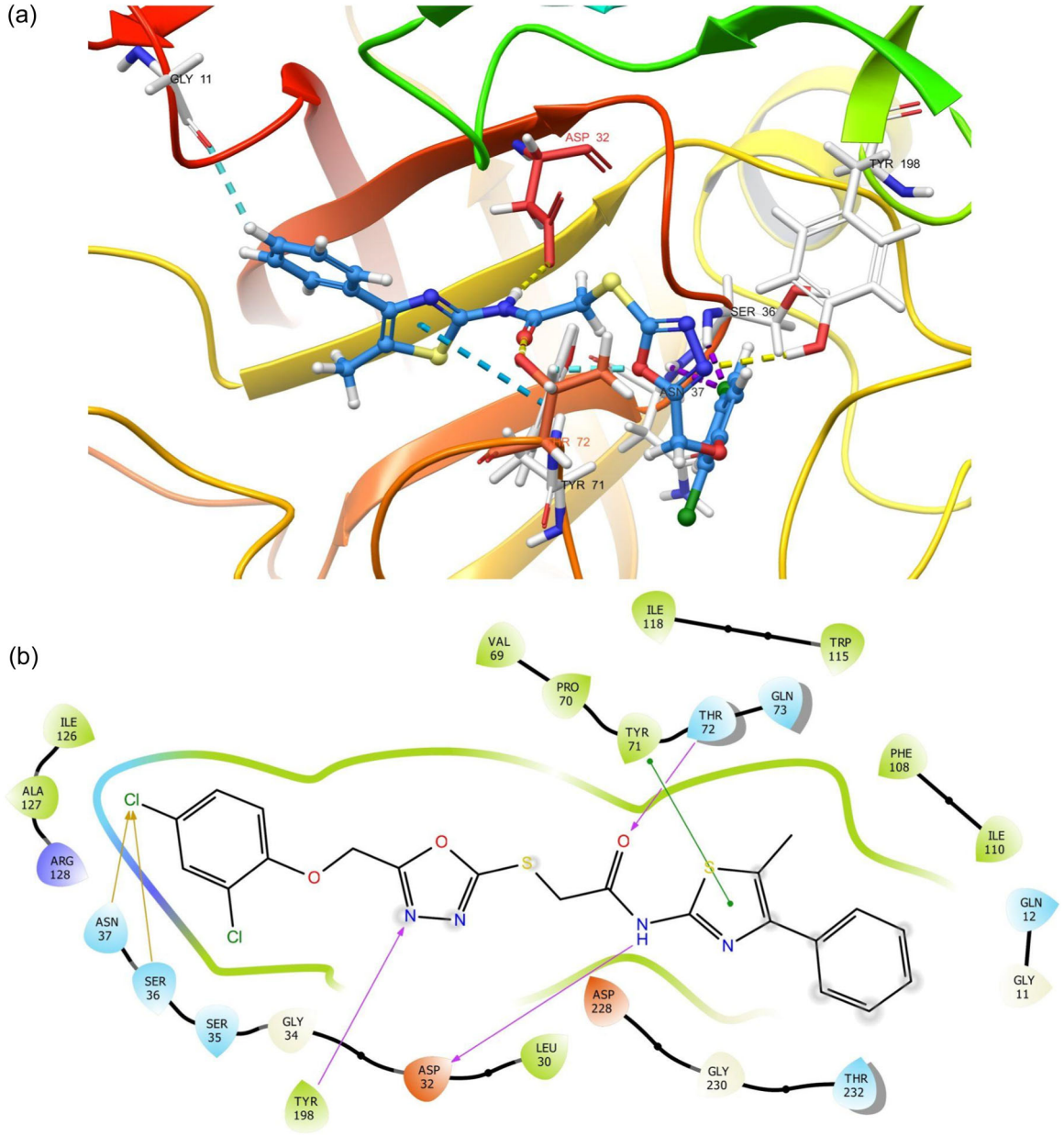

FIGURE 6 Best docking pose of compound **7e** in active pocket of the β-secretase enzyme (PDBID: 2ZJM). (a) 3D and (b) 2D poses of **7e**-BACE-1 complex. For the clarity, only interacted residues were showed. Red carbons represent key residues, other binding residues have white carbons.

1.79 Å for the protein while root-mean-square fluctuation (RMSF) plot was obtained as expected and the fluctuations of interacted residues were measured under 1.0 Å even for the loop amino acids. Because of these indicators, the stability properties (Figure 7a–c) were acceptable as described previously.[29,30]

Figure 7d–f and Video S1 indicated that interactions with Asp74, Phe295, and Phe286 residues have a major role in inhibitory activity and the protection of the stability of the enzyme. In Video S1, white carbons were used for the interacted residues, red carbons were used for the key amino acids, and violet carbons were used for highlighting the residues that formed halogen bonds with **7a**. Specifically, Trp86 (CAS) and Trp286 (PAS) are defined as key amino acids previously.[31,32] Our findings indicated that the inhibitory activity was more related to Trp286 (PAS) than Trp86 (CAS) directly. However, it has been revealed that 2,4-dichlorophenoxy group connected to some loop amino acids (seq. Gly120, Gly121, Tyr133, Glu202) via halogen bonding in CAS while it also stacked with His447 and Tyr449 in this region. Additionally, it formed halogen bonds with Tyr337 and Tyr341. All these amino acids increased the complex stability in CAS, thus, we portend that the stability was protected indirectly, too, even though the direct interactions with Trp86 were not stable during the simulation. In particular, it was observed that water-mediated interactions with Asp74, Ser293, and Phe295 residues were formed and also protected, therefore, in this case,

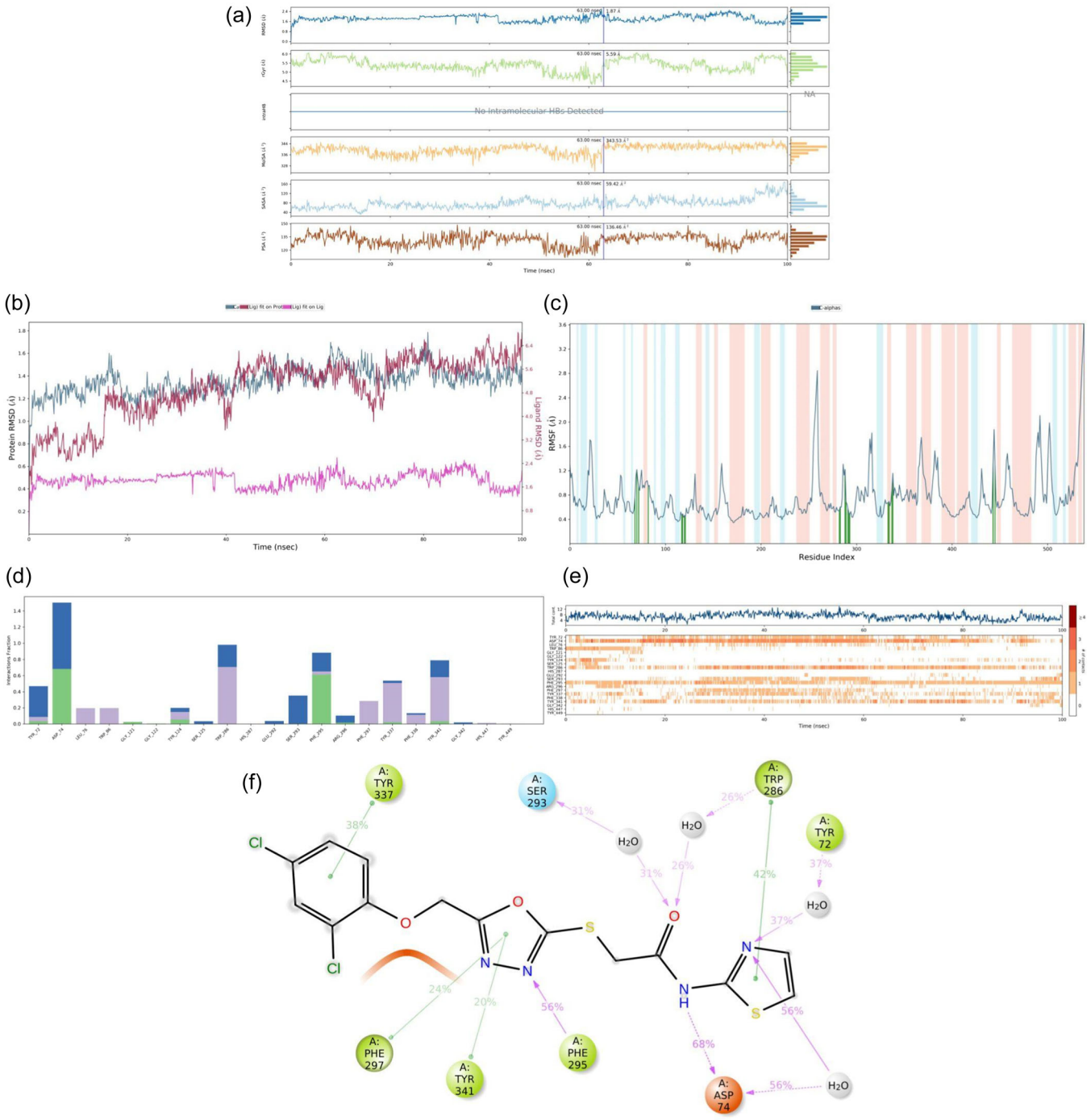

FIGURE 7 Molecular dynamics simulations (MDS) plots of **7a**-acetylcholinesterase (AChE) enzyme complex. (a) Ligand properties diagram, (b) root-mean-square deviation (RMSD) plot of ligand and protein during the simulation, (c) root-mean-square fluctuation (RMSF) plot of amino acids with the interactions, (d) interaction fraction-residue diagram, (e) number of interactions–interaction types-time plot, (f) total connections-residues-time plot (cutoff = 20%).

we suggest that water molecules played an important role in forming halogen and hydrogen bonds. Meanwhile, aromatic H-bonds were also observed with CAS region amino acids (seq. Gly120, Gly121, Tyr133, Glu202, His447, and Tyr449 as shown in Video S1). These connections were not stable as much as water-mediated H-bonds, still, it can be concluded that they contributed stability of the complex. Briefly, as suggested in the docking section, 2,4-dichlorophenoxy moiety was a notable pharmacophoric group to fit in the CAS region due to the halogen bonding and stacking π–π ability. As oxadiazole, the center of the compound, was forming H bond and π–π stacking with loop region (seq. 289–311) and π–π stacking with also alfa-helix residues (seq. 335–342), it increased stability of the complex which resulted in observing the inhibitory activity.

2.6.2 | BACE-1 inhibitory activity

The plots for stability properties and interaction profile were shared in Figure 8a–e for MDS study. rG values were observed without drastic changed which shows the complex is stable. RMSD value of protein were observed at 1.87 Å as the highest during the entire simulation, meanwhile, RMSF plot was obtained as expected and the fluctuations of interacted residues were measured under 1.0 Å even for the loop amino acids. These three plots showed that the stability of the complex was protected for the whole simulation, and thus, the interaction plots are trustable.

According to Figure 8d–f and Video S2, direct, aromatic, and water-mediated H-bonds seen frequently with Aps32, Gly34, Thr72, Gln73, Tyr198, Gly230, THR231, and Arg235. Similar to its docking pose, 2,4-dichlorophenoxy moiety of **7e** extended in S2' pocket of

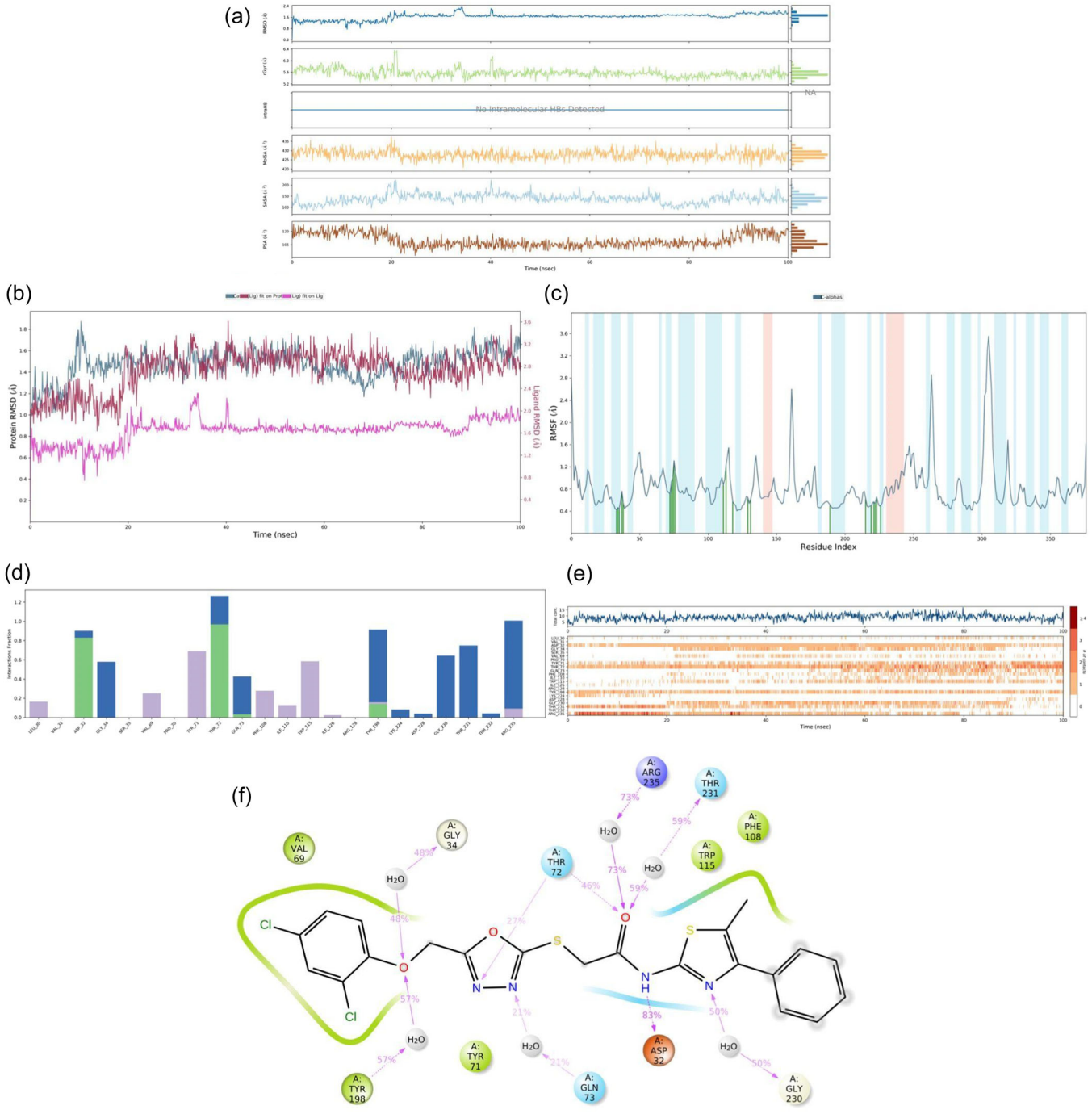

FIGURE 8 Molecular dynamics simulations (MDS) plots of **7a**-acetylcholinesterase (AChE) enzyme complex. (a) Ligand properties diagram, (b) root-mean-square deviation (RMSD) plot of ligand and protein during the simulation, (c) root-mean-square fluctuation (RMSF) plot of amino acids with the interactions, (d) interaction fraction-residue diagram, (e) number of interactions-interaction types-time plot, (f) total connections-residues-time plot (cutoff = 20%).

BACE-1 enzyme (Video S2), but interacted with Pro70 and Arg128 instead of Ser36 and Asn37. We're reporting that the 2,4-dichlorophenoxy ring positively affected the complex stability due to holding three loop regions in S2' pocket. Also, instead of the oxadiazole ring, MDS indicated importantly that oxygen of 2,4-dichlorophenoxy moiety formed water-mediated H-bond with Tyr198 residue. And this oxygen also formed water-mediated H-bond with Gly34. These findings indicated that this side of the ligand increased complex stability. On the other hand, nitrogens of oxadiazole ring formed H bonds with Thr72 (direct) and Gln73 (water-mediated) when the linker, acetamide, formed H-bonds with Asp35 (direct), Thr231 (water-mediated) and Arg235 (water-mediated). The nitrogen of thiazole formed water mediated H-bond with Gly230 which is a member of S3 subpocket and one of the important key residues.[33] Moreover, phenyl and methyl substitutions on thiazole occupied this subpocket, therefore, the active pocket was fulfilled by **7e**. All these findings indicated that bulky groups are more favor in inhibiting β-secretase enzyme.

3 | CONCLUSIONS

This study focused on the synthesis and evaluation of 11 newly synthesized compounds as potential anti-Alzheimer disease. The compounds were assessed for their inhibitory activity against AChE and BChE. Among the tested compounds, derivatives **6d**, **7a**, and **7e** demonstrated significant inhibitory effects on AChE, with IC_{50} values of 0.120, 0.039, and 0.063 μM, respectively while **7e** (IC_{50}: 0.123 μM) was also inhibit BACE-1 enzyme. These compounds exhibited close potential to the standard drug donepezil. However, the compounds showed limited effectiveness against BChE, with only four compounds exhibiting more than 40% inhibition at higher concentrations. Structural analysis revealed that compounds **6a–f** contained substituted benzothiazole, while compounds **7a–e** contained substituted thiazole, with **6d**, **7a**, and **7e** displaying the highest inhibitory activity within their respective groups. Computational studies using density functional theory (DFT) provided insights into the stability and reactivity of the active compounds, with compound **6d** showing enhanced electrophilic character and compound **7e** demonstrating nucleophilic character. These findings contribute to the understanding of the structure–activity relationship and provide valuable insights for the design of anticholinesterase agents.

4 | MATERIALS AND METHODS

4.1 | Chemistry

4.1.1 | General

All chemicals used in the syntheses were purchased either from Merck Chemicals (Merck KGaA) or Sigma-Aldrich Chemicals (Sigma-Aldrich Corp.). The reactions and the purities of the compounds were observed by thin layer chromatography (TLC) on silica gel 60 F254 aluminum sheets obtained from Merck (Darmstadt). The melting points of the synthesized compounds were recorded by the MP90 digital melting point apparatus (Mettler Toledo) and presented as uncorrected. ^{1}H-NMR and ^{13}C-NMR spectra (see the Supporting Information) were recorded by a Bruker 300 and 75 MHz digital FT-NMR spectrometer (Bruker Bioscience) in DMSO-d_6, respectively. In the NMR spectra, splitting patterns were designated as follows: s: singlet; d: doublet; t: triplet; m: multiplet. Coupling constants (*J*) were reported as Hertz. High-resolution mass spectrometric (HRMS) studies were performed using an LC/MS-IT-TOF system (Shimadzu, Kyoto, Japan). Elemental analyses were performed on a Leco 932 CHNS analyzer (Leco).

The InChI codes of the investigated compounds are provided as Supporting Information.

4.1.2 | Synthesis of methyl 2-(2,4-dichlorophenoxy) acetate (**1**)

2-(2,4-Dichlorophenoxy)acetic acid (18.10 mmol, 4 g) was dissolved in methanol, and 1 mL of sulfuric acid was added to the mixture. The mixture was stirred for 72 h at 65°C. The reaction control was checked by TLC. After the completion of the reaction, the crude product was obtained by evaporation of the solvent and then recrystallized from ethanol. Yield 91%.

4.1.3 | Synthesis of 2-(2,4-dichlorophenoxy) acetohydrazide (**2**)

Methyl 2-(2,4-dichlorophenoxy)acetate (**1**) (8.51 mmol, 2 g) and hydrazine hydrate (34 mmol of 85% 1.65 mL) were stirred at room temperature overnight in ethanol (100 mL). After TLC control, the mixture stopped stirring and waited for two phases of solvent and precipitate to form. The precipitated material was filtered. After drying, it was recrystallized with ethanol. Yield 84%.

4.1.4 | Synthesis of 5-[(2,4-dichlorophenoxy) methyl]-1,3,4-oxadiazole-2-thiol (**3**)

2-(2,4-Dichlorophenoxy)acetohydrazide (**2**) (12.76 mmol, 3 g) was dissolved in ethanol (50 mL) and the solution of potassium hydroxide (19.14 mmol, 0.77 g) in ethanol (40 mL) was added. After the addition of carbon disulfide (1.15 mL), the mixture refluxed for 6 h. After completion of the reaction, the solution was poured into ice water and acidified to pH 5–6 with dilute HCl to remove the salt form of the compound. The product (**3**) was filtered and dried. Yield 75%.

4.1.5 | General synthesis of *N*-(benzo[*d*]thiazol-2-yl)-2-chloroacetamide derivatives (**4**) and 2-chloro-*N*-(thiazol-2-yl)acetamide derivatives (**5**)

The compound's benzo[d]thiazol-2-amine derivatives and thiazol-2-amine derivatives were solved in tetrahydrofuran (THF), and triethylamine was used as a catalyst. The final mixture was cooled on an ice bed, and then 2-chloroacetyl chloride diluted in tetrahydrofuran was cautiously added dropwise to the solution. The mixture was stirred at room temperature for another 2 h after the addition of 2-chloroacetyl chloride. The reaction was controlled by TLC. After completion of the reaction, the solvent was evaporated, and the solid product was washed with water and filtered. Subsequently, the crude product was recrystallized from ethanol.

4.1.6 | General synthesis of *N*-(benzo[*d*]thiazol-2-yl)-2-({5-[(2,4-dichlorophenoxy)methyl]-1,3,4-oxadiazol-2-yl}thio)acetamide derivatives (**6**) and 2-({5-[(2,4-dichlorophenoxy)methyl]-1,3,4-oxadiazol-2-yl}thio)-*N*-(thiazol-2-yl)acetamide derivatives (**7**)

N-(Benzothiazol-2-yl)-2-chloroacetamide derivatives (**4**) and 2-chloro-*N*-(thiazol-2-yl)acetamide derivatives (**5**) (1.08 mmol) were added to a solution of 5-((2,4-dichlorophenoxy)methyl)-1,3,4-oxadiazole-2-thiol (**3**) (1.08 mmol, 0.3 g) in acetone (25 mL). K_2CO_3 (1.62 mmol, 0.22 g) was added to the mixture, and the mixture was stirred for 6 h at room temperature. The reaction was monitored with TLC (EtOAc/PET = 1:3). After the reaction was completed, acetone was removed, and the crude product was washed with water and recrystallized from ethanol.

N-(Benzo[d]thiazol-2-yl)-2-({5-[(2,4-dichlorophenoxy)methyl]-1,3,4-oxadiazol-2-yl}thio)acetamide (**6a**): m.p. 185–186°C, yield 77%, ^{1}H-NMR (300 MHz, DMSO-d_6, ppm) δ 4.20 (s, 2H, S-$\underline{CH_2}$), 5.52 (s, 2H, O-$\underline{CH_2}$), 7.07 (t, J = 7.81 Hz, 1H, Ar-H), 7.24 (t, J = 7.86 Hz, 1H, Ar-H), 7.36 (d, J = 8.95 Hz, 1H, Ar-H), 7.44 (d, J = 8.92 Hz, 1H, Ar-H) 7.50 (d, J = 7.84 Hz, 1H, Ar-H) 7.62 (d, J = 2.48 Hz, 1H, Ar-H) 7.71 (d, J = 7.68 Hz, 1H, Ar-H). ^{13}C-NMR (75 MHz, DMSO-d_6, ppm) δ 39.83 (S-$\underline{CH_2}$), 61.11 (O-$\underline{CH_2}$), 116.62, 119.47, 121.31, 121.52, 123.32, 125.06, 126.42, 128.68, 130.04, 133.08, 150.53, 152.26, 163.02, 166.46, 169.94. HRMS (*m/z*): $[M+H]^+$ calculated 466.9801; found 466.9812.

2-({5-[(2,4-Dichlorophenoxy)methyl]-1,3,4-oxadiazol-2-yl}thio)-*N*-(6-methoxybenzo[*d*]thiazol-2-yl)acetamide (**6b**): m.p. 203–204°C, yield 84%, ^{1}H-NMR (300 MHz, DMSO-d_6, ppm) δ 3.81 (s, 3H, O-$\underline{CH_3}$), 4.45 (s, 2H, S-$\underline{CH_2}$), 5.52 (s, 2H, O-$\underline{CH_2}$), 7.05 (d, J = 8.87 Hz, 1H, Ar-H), 7.33 (d, J = 8.95 Hz, 1H, Ar-H), 7.42 (d, J = 8.90 Hz, 1H, Ar-H), 7.58–7.60 (m, 2H, Ar-H), 7.67 (d, J = 8.85 Hz, 1H, Ar-H) 12.66 (brs, 1H, -$\underline{NH}$). ^{13}C-NMR (75 MHz, DMSO-d_6, ppm) δ 36.07 (S-$\underline{CH_2}$), 56.10 (O-$\underline{CH_3}$), 61.05 (O-$\underline{CH_2}$), 105.17, 115.55, 116.50, 121.80, 126.45, 128.65, 130.02, 133.23, 152.19, 156.72, 163.66, 164.93, 166.30. HRMS (*m/z*): $[M+H]^+$ calculated 496.9906; found 496.9947.

N-(6-Chlorobenzothiazol-2-yl)-2-({5-[(2,4-dichlorophenoxy)methyl]-1,3,4-oxadiazol-2-yl}thio)acetamide (**6c**): m.p. 195–196°C, yield 81%, ^{1}H-NMR (300 MHz, DMSO-d_6, ppm) δ 4.39 (s, 2H, S-$\underline{CH_2}$), 5.51 (s, 2H, O-$\underline{CH_2}$), 7.34 (d, J = 8.95 Hz, 1H, Ar-H), 7.39–7.43 (m, 2H, Ar-H), 7.60 (s, 1H, Ar-H), 7.69 (d, J = 8.63 Hz, 1H, Ar-H), 8.04 (s, 1H, Ar-H). ^{13}C-NMR (75 MHz, DMSO-d_6, ppm) δ 37.11 (S-$\underline{CH_2}$), 61.07 (O-$\underline{CH_2}$), 116.53, 121.64, 121.86, 123.28, 126.55, 127.46, 128.65, 130.01, 133.95, 152.21, 163.51.

2-({5-[(2,4-Dichlorophenoxy)methyl]-1,3,4-oxadiazol-2-yl}thio)-*N*-(6-nitrobenzothiazol-2-yl)acetamide (**6d**): m.p. 214–215°C, yield 86%, ^{1}H-NMR (300 MHz, DMSO-d_6, ppm) δ 4.34 (s, 2H, S-$\underline{CH_2}$), 5.52 (s, 2H, O-$\underline{CH_2}$), 7.35 (d, J = 8.94 Hz, 1H, Ar-H), 7.43 (d, J = 8.86 Hz, 1H, Ar-H), 7.60 (s, 1H, Ar-H), 7.69 (d, J = 8.93 Hz, 1H, Ar-H), 8.18 (d, J = 8.94 Hz, 1H, Ar-H), 8.82 (s, 1H, Ar-H). ^{13}C-NMR (75 MHz, DMSO-d_6, ppm) δ 38.56 (S-$\underline{CH_2}$), 61.08 (O-$\underline{CH_2}$), 116.56, 118.55, 119.55, 121.65, 123.29, 126.42, 128.65, 130.00, 133.21, 141.96, 152.22, 155.71, 163.31, 165.72, 170.63. HRMS (*m/z*): $[M+H]^+$ calculated 511.9651; found 511.9662.

2-({5-[(2,4-Dichlorophenoxy)methyl]-1,3,4-oxadiazol-2-yl}thio)-*N*-(6-methylbenzo[*d*]thiazol-2-yl)acetamide (**6e**): m.p. 215–216°C, yield 77%, ^{1}H-NMR (300 MHz, DMSO-d_6, ppm) δ 2.41 (s, 3H, Ar-$\underline{CH_3}$), 4.45 (s, 2H, S-$\underline{CH_2}$), 5.51 (s, 2H, O-$\underline{CH_2}$), 7.26 (d, J = 8.41 Hz, 1H, Ar-H), 7.33 (d, J = 8.96 Hz, 1H, Ar-H), 7.38–7.43 (m, 1H, Ar-H), 7.58–7.66 (m, 2H, Ar-H), 7.77 (s, 1H, Ar-H), 12.71 (brs, 1H, -$\underline{NH}$). ^{13}C-NMR (75 MHz, DMSO-d_6, ppm) δ 21.44 (Ar-$\underline{CH_3}$), 36.12 (S-$\underline{CH_2}$), 61.05 (O-$\underline{CH_2}$), 116.51, 120.80, 121.80, 123.27, 126.45, 128.03, 128.65, 130.05, 132.04, 133.72, 152.19, 152.31, 163.66, 164.92, 166.48.

2-({5-[(2,4-Dichlorophenoxy)methyl]-1,3,4-oxadiazol-2-yl}thio)-*N*-(6-ethoxybenzo[*d*]thiazol-2-yl)acetamide (**6f**): m.p. 185–186°C, yield 71%, ^{1}H-NMR (300 MHz, DMSO-d_6, ppm) δ 1.34 (t, J = 6.93 Hz, 3H, O-CH$_2$-$\underline{CH_3}$), 4.06 (q, J = 6.95 Hz, 2H, O-$\underline{CH_2}$-CH$_3$), 4.42 (s, 2H, S-$\underline{CH_2}$), 5.51 (s, 2H, O-$\underline{CH_2}$), 7.02 (d, J = 8.82 Hz, 1H, Ar-H), 7.33 (d, J = 8.95 Hz, 1H, Ar-H), 7.41 (d, J = 8.88 Hz, 1H, Ar-H), 7.53 (s, 1H, Ar-H). 7.58–7.61 (m, 1H, Ar-H), 7.64 (s, 1H, Ar-H). ^{13}C-NMR (75 MHz, DMSO-d_6, ppm) δ 15.16 (O-CH$_2$-$\underline{CH_3}$), 36.32 (S-$\underline{CH_2}$), 61.06 (O-$\underline{CH_2}$), 64.04 (O-$\underline{CH_2}$-CH$_3$), 105.75, 115.73, 116.52, 121.64, 123.28, 126.44, 128.64, 130.00, 133.29, 152.19, 155.82, 163.61, 165.05, 166.51. HRMS (*m/z*): $[M+H]^+$ calculated 511.0063; found 511.0025.

2-({5-[(2,4-Dichlorophenoxy)methyl]-1,3,4-oxadiazol-2-yl}thio)-*N*-(thiazol-2-yl)acetamide (**7a**): m.p. 180–181°C, yield 80%, ^{1}H-NMR (300 MHz, DMSO-d_6, ppm) δ 4.40 (s, 2H, S-$\underline{CH_2}$), 5.51 (s, 2H, O-$\underline{CH_2}$), 7.25 (d, J = 3.60 Hz, 1H, Ar-H), 7.34 (d, J = 8.94 Hz, 1H, Ar-H), 7.42 (d, J = 8.88 Hz, 1H, Ar-H), 7.50 (d, J = 3.57 Hz, 1H, Ar-H), 7.61 (s, 1H, Ar-H). ^{13}C-NMR (75 MHz, DMSO-d_6, ppm) δ 35.99 (S-$\underline{CH_2}$), 61.05 (O-$\underline{CH_2}$), 114.25, 116.52, 123.29, 126.46, 128.65, 130.05, 138.19, 152.19, 158.51, 163.59, 165.01, 165.57. HRMS (*m/z*): $[M+H]^+$ calculated 416.9644; found 416.9670.

2-({5-[(2,4-Dichlorophenoxy)methyl]-1,3,4-oxadiazol-2-yl}thio)-*N*-(4-methylthiazol-2-yl)acetamide (**7b**): m.p. 150–151°C, yield 88%, ^{1}H-NMR (300 MHz, DMSO-d_6, ppm) δ 2.30 (s, 3H, thiazole-$\underline{CH_3}$),

4.29 (s, 2H, S-$\underline{CH_2}$), 5.51 (s, 2H, O-$\underline{CH_2}$), 7.06 (s, 1H, Ar-H), 7.34 (d, J = 8.94 Hz, 1H, Ar-H), 7.42 (d, J = 8.89 Hz, 1H, Ar-H), 7.61 (s, 1H, Ar-H). ^{13}C-NMR (75 MHz, DMSO-d_6, ppm) δ 11.87 (thiazole-$\underline{CH_3}$), 37.29 (S-$\underline{CH_2}$), 61.06 (O-$\underline{CH_2}$), 116.54, 123.30, 125.54, 126.43, 128.65, 130.00, 130.04, 134.92, 152.21, 160.05, 163.35, 165.59, 166.03. HRMS (m/z): $[M+H]^+$ calculated 430.9801; found 430.9822.

2-({5-[(2,4-Dichlorophenoxy)methyl]-1,3,4-oxadiazol-2-yl}thio)-*N*-(4-phenylthiazol-2-yl)acetamide (**7c**): m.p. 184–185°C, yield 79%, ^{1}H-NMR (300 MHz, DMSO-d_6, ppm) δ 4.19 (s, 2H, S-$\underline{CH_2}$), 5.51 (s, 2H, O-$\underline{CH_2}$), 7.23 (d, J = 10.60 Hz, 2H, Ar-H), 7.34–7.41 (m, 4H, Ar-H), 7.43–7.61 (m, 1H, Ar-H), 7.88 (d, J = 7.34 Hz, 1H, Ar-H). ^{13}C-NMR (75 MHz, DMSO-d_6, ppm) δ 40.10 (S-$\underline{CH_2}$), 61.12 (O-$\underline{CH_2}$), 106.36, 116.61, 123.32, 125.96, 126.43, 127.22, 128.67, 128.84, 130.00, 130.05, 136.22, 148.31, 152.26, 163.00, 166.55, 167.39, 168.46. HRMS (m/z): $[M+H]^+$ calculated 492.9957; found 492.9983.

Ethyl 2-[2-({5-[(2,4-Dichlorophenoxy)methyl]-1,3,4-oxadiazol-2-yl}thio)acetamid]-4-methylthiazole-5-carboxylate (**7d**): m.p. 180–181°C, yield 85%, ^{1}H-NMR (300 MHz, DMSO-d_6, ppm) δ 1.25 (t, J = 7.10 Hz, 3H, O-CH$_2$-$\underline{CH_3}$), 2.47 (s, 3H, thiazole-$\underline{CH_3}$), 4.13–4.20 (m, 4H, O-$\underline{CH_2}$-CH$_3$ and S-$\underline{CH_2}$), 5.51 (s, 2H, O-$\underline{CH_2}$), 7.35 (d, J = 8.95 Hz, 1H, Ar-H), 7.43 (d, J = 8.88 Hz, 1H, Ar-H), 7.62 (s, 1H, Ar-H). ^{13}C-NMR (75 MHz, DMSO-d_6, ppm) δ 14.84 (O-CH$_2$-$\underline{CH_3}$), 17.90 (thiazole-$\underline{CH_3}$), 39.19 (S-$\underline{CH_2}$), 59.96 (O-$\underline{CH_2}$-CH$_3$), 61.09 (O-$\underline{CH_2}$), 111.02, 116.60, 123.32, 126.42, 128.66, 130.00, 152.24, 157.20, 163.09, 163.33, 166.18, 169.98. HRMS (m/z): $[M+H]^+$ calculated 503.0012; found 503.0024.

2-({5-[(2,4-Dichlorophenoxy)methyl]-1,3,4-oxadiazol-2-yl}thio)-*N*-(5-methyl-4-phenylthiazol-2-yl)acetamide (**7e**): m.p. 171–172°C, yield 77%, ^{1}H-NMR (300 MHz, DMSO-d_6, ppm) δ 2.46 (s, 3H, thiazole-$\underline{CH_3}$), 4.35 (s, 2H, S-$\underline{CH_2}$), 5.52 (s, 2H, O-$\underline{CH_2}$), 6.78 (s, 1H, Ar-H), 7.35 (t, J = 5.01 Hz, 1H, Ar-H), 7.38–7.41 (m, 1H, Ar-H), 7.45 (t, J = 7.22 Hz, 2H, Ar-H), 7.56 (d, J = 7.07 Hz, 1H, Ar-H), 7.61 (d, J = 2.55 Hz, 1H, Ar-H), 7.64 (d, J = 7.08 Hz, 1H, Ar-H). ^{13}C-NMR (75 MHz, DMSO-d_6, ppm) δ 12.49 (thiazole-$\underline{CH_3}$), 36.50 (S-$\underline{CH_2}$), 61.05 (O-$\underline{CH_2}$), 116.52, 121.36, 123.30, 126.44, 127.15, 127.58, 128.42, 128.57, 128.65, 128.79, 130.02, 135.53, 152.20, 163.51, 165.23, 165.91. HRMS (m/z): $[M+H]^+$ calculated 507.0114; found 507.0144.

4.2 | Biological assays

4.2.1 | AChE and BChE inhibition

Compounds **6a–f** and **7a–e** were tested on AChE and BChE enzymes to determine their anticholinesterase effects. The study was performed according to the Ellman method[34] and the results are presented as percent inhibition and inhibition concentration in μM. Human AChE (CAS No: 9000-81-1) and human BChE (CAS No: 9001-08-5) enzymes were used in the experiment, and the results were compared with donepezil and tacrine molecules as standard drugs. After the compounds were tested at 10^{-3} M and 10^{-4} M concentrations, lower concentrations were started for compounds with high inhibitory properties. All tests were performed in triplicate. The experiment was conducted as stated in our previous study.[25]

4.2.2 | β-Secratase inhibition activity

The experimental procedure was based on the "Human β-Secretase (BACE-1) Inhibitor Screening Assay" kit (Human β-Secretase (BACE1) Inhibitor Screening Kit (Fluorometric)-Catalog no:K720-100) protocol based on the fluorometric method as performed previously.[35]

4.3 | ADME parameters

Eleven final compounds were evaluated for their physicochemical properties, pharmacokinetics, and medicinal chemistry. The number of H-bond acceptors (NBA), number of H-bond donors (NBD), topological polar surface area (TPSA), partition coefficient (Log P), water solubility (Log S), gastrointestinal absorption (GI) level, skin permeation (Log Kp), violation of Rule of Five (RoF), and synthetic accessibility (SA) were predicted, virtually. SwissADME was used for calculations, which is a free, quick, and reliable web tool utilized for in silico drug discovery studies.[36]

4.4 | Theoretical details

The Gaussian 09 W software package[37] and GaussView 5.0 molecular visualization program[38] were used for the theoretical analysis of the most active compounds, namely **6d**, **7a**, and **7e**. DFT with Becke's Three-Parameter Hybrid Functional and the Lee, Yang, and Parr correlation (B3LYP) method[39] was employed to optimize the compounds' geometry in the ground state and gas phase, using the 6-31 G(d,p) basis set. To investigate intramolecular charge-transfer interactions, time-dependent (TD)-DFT calculations were performed to obtain the highest occupied molecular orbital (HOMO) and lowest unoccupied molecular orbital (LUMO) energy values for the compound groups. These energy values were then used to derive various chemical activity parameters such as ionization potential (I = −E HOMO), electron affinity (A = −ELUMO), electronegativity (χ = (I + A)/2), chemical hardness (η = (I − A)/2), chemical softness (S = 1/2η), chemical potential (μ = −(I + A)/2), and electrophilicity index (ω = μ2/2η) of the molecular groups.[40–44]

4.5 | In silico studies

The in-silico docking studies were conducted using the Schrodinger Maestro Suite program, which provided a robust platform for protein and ligand preparation, grid generation, docking, and visualization. Crystal structures of the enzymes were retrieved from the Protein Data Bank server (PDBID: 4EY7 and 2ZJM, respectively), with all ligands adjusted to physiological pH during protonation. Proteins underwent preparation according to established protocols.[26,27,40,45–48] Molecular dynamics simulations (MDS) were executed via the Maestro Desmond interface program, each running for 100 ns to assess stability. System setup, MDS, and interaction

analysis followed standardized procedures. Energy minimization leveraging the OPLS3e force field was performed using "System Builder" in Maestro. The hydration model employed the transferable intermolecular potential with the 3-point water model, and system neutralization utilized Na+ and Cl− ions. Molecular dynamic simulations included calculations of radius of gyration (Rg), root-mean-square fluctuation (RMSF), and root-mean-square deviation (RMSD) via the Desmond application.[29,49,50]

Furthermore, the in-silico docking procedure aimed to elucidate potential ligand interactions with acetylcholinesterase and β-secretase enzymes (PDBID: 4EY7 and 2ZJM, respectively). Docking studies were performed for compounds **6d**, **7a**, and **7e** within the AChE active pocket and BACE-1 binding cavity. Subsequently, compound **7e**, identified as the most active on both enzymes, underwent MDS for 100 ns to assess stability and behavior, following established protocols.

ACKNOWLEDGMENTS

We would like to thank to Anadolu University BİBAM and MERLAB for spectroscopic analysis.

CONFLICTS OF INTEREST STATEMENT

The authors declare no conflicts of interest.

DATA AVAILABILITY STATEMENT

The data that supports the findings of this study are available in the Supporting Information of this article.

ORCID

Asaf E. Evren https://orcid.org/0000-0002-8651-826X
Demokrat Nuha http://orcid.org/0000-0002-7271-6791
Leyla Yurttaş http://orcid.org/0000-0002-0957-6044

REFERENCES

[1] M. Zvěřová, *Clin. Biochem*. **2019**, *72*, 3.
[2] P. Kamat, *Neural Regen. Res*. **2015**, *10*, 1050.
[3] Alzheimer's Association. *Alzheimer's Dement*. **2015**, *11*(2015), 332.
[4] Alzheimer's Association. *Alzheimer's Dement*. **2018**, *14*, 367.
[5] H. Hampel, J. Hardy, K. Blennow, C. Chen, G. Perry, S. H. Kim, V. L. Villemagne, P. Aisen, M. Vendruscolo, T. Iwatsubo, C. L. Masters, M. Cho, L. Lannfelt, J. L. Cummings, A. Vergallo, *Mol. Psychiatry* **2021**, *26*, 5481.
[6] Q. Jia, Y. Deng, H. Qing, *BioMed Res. Int*. **2014**, *2014*, 837157.
[7] R. P. Friedrich, K. Tepper, R. Rönicke, M. Soom, M. Westermann, K. Reymann, C. Kaether, M. Fändrich, *Proc. Natl. Acad. Sci. U.S.A*. **2010**, *107*, 1942.
[8] G. Marucci, M. Buccioni, D. D. Ben, C. Lambertucci, R. Volpini, F. Amenta, *Neuropharmacology* **2021**, *190*, 108352.
[9] M. D. Costa, B. M. Gai, C. I. Acker, A. C. G. Souza, R. Brandão, C. W. Nogueira, *Chem. Biol. Interact*. **2012**, *197*, 80.
[10] M. Simunkova, S. H. Alwasel, I. M. Alhazza, K. Jomova, V. Kollar, M. Rusko, M. Valko, *Arch. Toxicol*. **2019**, *93*, 2491.
[11] T. Tomofuji, D. Ekuni, T. Azuma, K. Irie, Y. Endo, K. Kasuyama, T. Yoneda, M. Morita, *Lipids. Health Dis*. **2013**, *12*, 1.
[12] J. A. Smith, A. Das, S. K. Ray, N. L. Banik, *Brain Res. Bull*. **2012**, *87*, 10.
[13] W. Y. Wang, M. S. Tan, J. T. Yu, L. Tan, *Ann. Transl. Med*. **2015**, *3*, 136.
[14] A. Iraji, M. Khoshneviszadeh, O. Firuzi, M. Khoshneviszadeh, N. Edraki, *Bioorg. Chem*. **2020**, *97*, 103649.
[15] L. Bharti, R. Kumar, B. Winblad, *Eur. J. Med. Chem*. **2021**, *209*, 112915.
[16] H. Zhang, Y. Wang, Y. Wang, X. Li, S. Wang, Z. Wang, *Eur. J. Med. Chem*. **2022**, *240*, 114606.
[17] H. Zhang, Y. Peng, L. Zhuo, Y. Wang, G. Zeng, S. Wang, L. Long, X. Li, Z. Wang, *Eur. J. Med. Chem*. **2022**, *242*, 114695.
[18] A. K. Saxena, *Alzheimer's Neurodegen. Dis*. **2019**, *4*, 1.
[19] H. Singh, J. V. Singh, K. Bhagat, H. K. Gulati, M. Sanduja, N. Kumar, N. Kinarivala, S. Sharma, *Bioorg. Med. Chem*. **2019**, *27*, 3477.
[20] R. S. Keri, K. Chand, S. Budagumpi, S. Balappa Somappa, S. A. Patil, B. M. Nagaraja, *Eur. J. Med. Chem*. **2017**, *138*, 1002.
[21] C. A. Lipinski, F. Lombardo, B. W. Dominy, P. J. Feeney, *Adv. Drug Deliv. Rev*. **1997**, *23*, 3.
[22] C. B. P. Kumar, M. S. Raghu, K. N. N. Prasad, S. Chandrasekhar, B. K. Jayanna, F. A. Alharthi, M. K. Prashanth, K. Y. Kumar, *New J. Chem*. **2021**, *45*, 403.
[23] P. Politzer, J. S. Murray, *Theor. Chem. Accounts Theory Comput. Model*. **2002**, *108*, 134.
[24] F. J. Luque, M. Orozco, P. K. Bhadane, S. R. Gadre, *J. Phys. Chem*. **2002**, *97*, 9380.
[25] Ş. Durmaz, A. E. Evren, B. N. Sağlık, L. Yurttaş, N. F. Tay, *Arch. Pharm*. **2022**, *355*, e2200294.
[26] A. A. Al-Sharabi, A. E. Evren, B. N. Sağlık, L. Yurttaş, *J. Biomol. Struct. Dyn*. **2023**, *41*, 1.
[27] B. N. Sağlık, S. Levent, D. Osmaniye, A. E. Evren, A. B. Karaduman, Y. Özkay, Z. A. Kaplancıklı, *ACS Omega* **2022**, *7*, 47378.
[28] D. Osmaniye, A. E. Evren, B. N. Sağlık, S. Levent, Y. Özkay, Z. A. Kaplancıklı, *Arch. Pharm*. **2022**, *355*, e2100450.
[29] A. E. Evren, A. B. Karaduman, B. N. Sağlik, Y. Özkay, L. Yurttaş, *ACS Omega* **2023**, *8*, 1410.
[30] A. E. Evren, D. Nuha, S. Dawbaa, B. N. Sağlık, L. Yurttaş, *Eur. J. Med. Chem*. **2022**, *229*, 114097.
[31] D. Iqbal, M. T. Rehman, A. Bin Dukhyil, S. M. D. Rizvi, M. F. Al Ajmi, B. M. Alshehri, S. Banawas, M. S. Khan, W. Alturaiki, M. Alsaweed, *Pharmaceuticals* **2021**, *14*, 937.
[32] A. Y. Hemaida, G. S. Hassan, A. R. Maarouf, J. Joubert, A. A. El-Emam, *ACS Omega* **2021**, *6*, 19202.
[33] C. R. Butler, K. Ogilvie, L. Martinez-Alsina, G. Barreiro, E. M. Beck, C. E. Nolan, K. Atchison, E. Benvenuti, L. Buzon, S. Doran, C. Gonzales, C. J. Helal, X. Hou, M. H. Hsu, E. F. Johnson, K. Lapham, L. Lanyon, K. Parris, B. T. O'Neill, D. Riddell, A. Robshaw, F. Vajdos, M. A. Brodney, *J. Med. Chem*. **2017**, *60*, 386.
[34] G. L. Ellman, K. D. Courtney, V. Andres, Jr., R. M. Feather-Stone, *Biochem. Pharmacol*. **1961**, *7*, 88.
[35] F. Tok, B. N. Sağlık, Y. Özkay, Z. A. Kaplancıklı, B. Koçyiğit-Kaymakçıoğlu, *J. Mol. Struct*. **2022**, *1265*, 133441.
[36] B. Bakchi, A. D. Krishna, E. Sreecharan, V. B. J. Ganesh, M. Niharika, S. Maharshi, S. B. Puttagunta, D. K. Sigalapalli, R. R. Bhandare, A. B. Shaik, *J. Mol. Struct*. **2022**, *1259*, 132712.
[37] M. Frisch, G. Trucks, H. Schlegel, G. Scuseria, M. Robb, J. Cheeseman, G. Scalmani, V. Barone, B. Mennucci, G. Petersson, *Gaussian09, Revision A*, Wallingford CT Inc. New York City **2009**, pp. 150.
[38] R. Dennington, T. Keith, J. Millam, GaussView, version 5, Wallingford CT Inc., New York City **2009**.
[39] A. D. Becke, *J. Chem. Phys*. **1992**, *96*, 2155.
[40] S. Dawbaa, D. Nuha, A. E. Evren, M. Y. Cankiliç, L. Yurttaş, G. Turan, *J. Mol. Struct*. **2023**, *1282*, 135213.
[41] D. Nuha, A. E. Evren, Ö. Kapusiz, Ü. D. Gül, N. Gundogdu-Karaburun, A. Ç. Karaburun, H. Berber, *J. Mol. Struct*. **2023**, *1272*, 134166.
[42] D. Nuha, A. E. Evren, Z. Ş. Çiyanci, H. E. Temel, G. Akalin Çiftçi, L. Yurttaş, *Arch. Pharm*. **2022**, *355*, e2200105.
[43] A. E. Evren, D. Nuha, L. Yurttaş, *Eur. J. Life Sci*. **2023**, *1*, 118.
[44] D. Nuha, H. Berber, A. Ç. Karaburun, *SSRN Electron. J*. **2022**. *25*, 10.

[45] S. Saffour, A. A. Al-Sharabi, A. E. Evren, M. Y. Cankiliç, L. Yurttaş, *J. Mol. Struct*. **2024**, *1295*, 136675.
[46] A. A. Al-Sharabi, S. Saffour, A. E. Evren, G. Bayazıt, G. Çongur, Ü. D. Gül, L. Yurttaş, *J. Mol. Struct*. **2023**, *1289*, 135775.
[47] S. A. Naji, B. N. Sağlik, M. Agamennone, A. E. Evren, N. Gundogdu-Karaburun, A. Ç. Karaburun, *ACS Omega* **2023**, *8*, 48884.
[48] S. Dawbaa, A. E. Evren, B. N. Sağlik, N. Gundogdu-Karaburun, A. C. Karaburun, *Future Med. Chem*. **2022**, *14*, 1663.
[49] A. E. Evren, D. Nuha, S. Dawbaa, A. B. Karaduman, B. N. Sağlik, L. Yurttaş, *J. Biomol. Struct. Dyn*. **2023**, *41*, 1.
[50] N. Turan Yücel, A. E. Evren, Ü. Kandemir, Ö. D. Can, *J. Psychopharmacol*. **2022**, *36*, 819.

SUPPORTING INFORMATION

Additional supporting information can be found online in the Supporting Information section at the end of this article.

How to cite this article: A. E. Evren, D. Nuha, B. N. S. Özkan, Ç. Kahraman, E. M. Gönülalan, L. Yurttaş, *Arch. Pharm*. **2024**;*357*:e2400115. https://doi.org/10.1002/ardp.202400115